



## Heat Transfer Enhancement Simulation Employing Flat and Curved Winglet Vortex Generator Pairs with Punched Holes

Saad Jabbar Nghaimesh\*<sup>ORCID</sup>, Mostafa Abbas Jabbar<sup>ORCID</sup>

Department of Mechanical Techniques, Al-Nasiriya Technical Institute, Southern Technical University, Al-Nasiriya 64001, Iraq

Corresponding Author Email: [saad.nghaimesh@stu.edu.iq](mailto:saad.nghaimesh@stu.edu.iq)

Copyright: ©2024 The authors. This article is published by IIETA and is licensed under the CC BY 4.0 license (<http://creativecommons.org/licenses/by/4.0/>).

<https://doi.org/10.18280/ijht.420518>

### ABSTRACT

**Received:** 11 April 2024

**Revised:** 14 September 2024

**Accepted:** 30 September 2024

**Available online:** 31 October 2024

#### Keywords:

heat transfer, vortex generators, curved winglets, punching holes

To comprehend heat transfer mechanisms, the study examines the flow and thermal characteristics of flat and curved vortex generators with punched holes on their surfaces.  $Re$  is varied from 3,000 to 18,000 in three-dimensional numerical simulations in a channel flow with two VGs mounted on the bottom wall. The improvement of heat transfer and pressure loss are investigated using the dimensionless parameters  $Num/Num_0$ ,  $f/f_0$ , and  $R = (Num/Num_0)/(f/f_0)$ . The results indicate that VGs with punched holes have higher  $Num/Num_0$  values compared to VGs without punched holes across all  $Re$  values. The most significant difference, up to 6.4%, is observed between VGs with openings (DWH) and VGs without punched holes (DWP) at  $Re=12,000$ . The apparent friction factor ( $f/f_0$ ), initially increases rapidly and then stabilizes with  $Re$ . The DWP has the highest friction factor  $f/f_0$ , ranging from 1.1 to 1.7, due to the larger area that confronts the airflow in the P-series of VGs, followed by DWH. Curved VGs CDW and CDWH are more effective in reducing drag and lowering  $f/f_0$  compared to plane VGs due to their streamlined shape. The jet flow from the perforations helps clear stagnant fluids and reduce pressure differences before and after the VGs. Also, the hydraulic heat capacity  $R$  is more effective in a curved VG than in a flat VG because of the improved heat transfer and lower wire flow. The thermo-hydraulic efficiency coefficient is determined by Colburn and friction coefficients, and CDWH has the highest resistance, followed by CDWP, DWH, and DWP. When  $Re=18,000$ , a rectangular VG with holes performs better than one without, with a maximum difference of 35.3%.

## 1. INTRODUCTION

In many modern projects, air-cooled heat exchangers (HXs) are used, especially in refrigeration, heating, ventilation, and air conditioning (Central air) systems. In any case, the air-side warm obstruction is generally high, which might represent (75-90%) of the absolute warm obstruction. As an inert force move overhaul device, vortex generators (VGs) have been widely used to further increase the air-side convective power move coefficient of finned tube type HXs and plate-sharp edge HXs. The conclusively situated VGs make assistant streams, especially longitudinal vortices that revolve around the mainstream going in a forward direction, upset the advancement of as far as a possible layer, convey the force from the wall to the focal point of the stream by progressing spinning development, and thusly lead to progress in heat move [1, 2]. A lot of thought has been given to the wings or winglets type of VGs, which can have a rectangular or three-sided construction, among other combinations. Nonetheless, with the increment of intensity move upgrade, the tension drop turns out to be enormous [3]. Tentatively concentrated on the intensity and stream execution of the Delta Winglet VGs on three-line HX finned tubes with a line and staggered tube game plan. The perspective proportion 2, 45° rake point VGs were

met by the balances some distance downstream of the cylinder in a downstream helpful design. The outcomes showed that the intensity move improvement was expanded by 55-65% and the comparing clear coefficient of grinding was expanded by 20-45% for in-line tubes [4].

Rectangular base vortex generators and top rib unpleasantness were utilized to expand the mean Nusselt number by practically 450%, however to the detriment of a strain drop of over 300% [5]. And led tests showing a 23-55% increment in heat move in tempestuous channel stream with three-sided and rectangular punctured VGs, bringing about a comparing pressure drop of 18-195% [6]. The capability of the VGs delta balance to further develop the air-side intensity move of the HX plain cylinder was assessed tentatively. The outcomes showed an improvement in heat movement somewhere in the range of 16.5% and 44% at a strain drop of 12% when the co-current direction was utilized [7]. The example was taken care of into rectangular VG microchannels to notice the historical backdrop of water development and power. The outcomes showed that fomentation force expanded by 9-21% in the laminar stream and 39-90% in the quick stream, while pressure drop expanded by 34-83% and 61-169%, separately. Further examinations were directed to notice the reduction in pressure and development force of the

microchannels [8]. Microchannels with aspect ratios of 0.0667 and 0.25 showed improvements in heat transfer performance of 12.3-73.8% and 3.4-45.4%, respectively, whereas pressure losses increased by 40.3-158.6% and 6.5-47.7%, respectively. According to the aforementioned studies, using VGs to improve heat transmission causes pressure loss to rise. Nevertheless, to enhance the overall performance factor  $R=(Nu/Nu_0)/(ff_0)$ , it is necessary to optimize the pressure loss [9]. It was observed that the VGs caused a significant amount of form drag, which resulted in a decrease in pressure. The liquid crystal thermography method was utilized to compare various wing-type VGs for their ability to enhance heat transfer [10]. The researchers discovered that the drag caused by VGs was almost directly related to the surface area and did not depend on the Reynolds number or the shape of the VGs. As the fluid passes over the barrier, it creates a region of slow recirculation behind it, causing damage and drag. Reducing form drag is important, and one way to do this is to reduce the area which also controls the circulation. To achieve this goal, the researchers investigated the sizes and consumption patterns of VGs using mathematical and experimental methods [11]. The installation of delta-winglet VGs in the "normal flow-on" system was found to increase heat transfer by 10-30% while reducing pressure losses in fin-tube heat exchangers by 34-55%. Completed the field is also [10]. 3-D numerical studies of wavy flow and heat transfer using novel vortex generators (VGs) such as curved angle rectangular winglets (CARW), angle rectangular winglets (ARW), and rectangular right-angle winglets (RTW) fin-tube are used and heat exchangers (HX) are used. According to the study, the RTW VGs were more successful in increasing the heat transfer at large angles of attack ranging from  $15^\circ$  to  $75^\circ$  [12].

The research investigates the effectiveness of curved delta wing vortex generators (CDWVG) with and without round holes in enhancing heat transfer in fin and tube heat exchangers (FTHEs) over a wide range of Reynolds numbers. This study analyzes the thermal-hydraulic performance of FTHE with different CDWVG configurations, including pressure distribution, temperature distribution, and flow structure. In addition, the study evaluated factors such as pressure drop, Nusselt number, and Colburn factor to evaluate the thermohydraulic performance of FTHE. The results show that the use of CDWVG with circular holes significantly improves the hydraulic thermal efficiency of the FTHE, with the 6-hole configuration being the most effective. In conclusion, implementing CDWVG improves heat transfer in FTHE [13]. The purpose of this study is to increase heat transmission in ducts by employing a pair of delta-camber perforated airfoils as vortex generators. Experiments included putting a vortex generator in a rectangular duct and varying the airflow speed. When a vortex generator was used for a three-row convex delta airfoil pair at a Reynolds number of 8,724, the Nusselt value ratio and friction factor ratio increased [14].

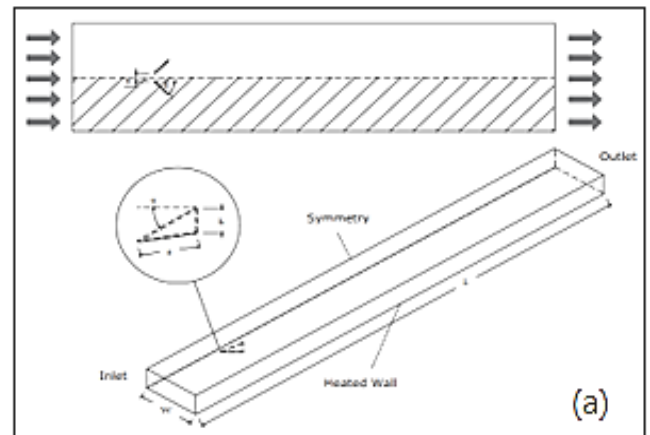
The study found that the Nusselt number increases at a 60-degree angle when examining convective heat transfer on flat plates and plates with delta winglet longitudinal vortex generators [15, 16]. Numerical simulations were used to investigate heat transfer and fluid flow in a flat-plate channel with longitudinal vortex generators, demonstrating that these generators improve heat transfer [17, 18].

## 2. MATHEMATIC MODEL AND PHYSICAL

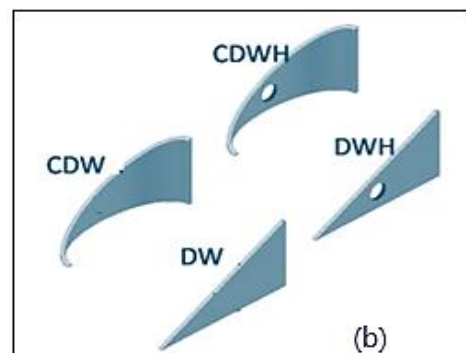
### 2.1 Physical model

The effects of different types of vertical vortex generators (VGs) on a rectangular air duct are investigated through 3-D numerical simulations. The VGs that were put through testing included flat VGs that were shaped like delta fin pairs (DWP) and delta fin pairs with holes (DWH), as well as curved VGs that were shaped like curved delta wing pairs with holes (CDWH) and curved delta fin pairs (CDWP), all of which were fastened to the duct's bottom wall. The surface being referred to is a semi-elliptical cylinder with a short-axis to the long-axis ratio of  $b/a=0.5$ . Punches have been created on different areas of the surface of these VGs with parameters such as  $l'$ ,  $a$ ,  $h'$ , and  $h''$ . These parameters denote the distance between the hole center and the trailing edge, the chord length of the VGs, and the height of the VG line going through the distance from the hole center to the bottom edge and the center of the hole, respectively. The punches were made at various locations with ratios of  $l'/a=1/3, 1/2, 2/3$  and  $h''/h'=1/3, 1/2, 2/3$ . The VGs without any holes are known as DWP and CDWP, which are the VGs with punched holes are known as DWH and CDWH as shown in Figure 1(a), 1(b).

VG configurations and geometric parameters are shown in the Figure 1(a) and Table 1. The computational domain with a built-in winglet pair is shown in the Figure 1(b), described in Cartesian coordinates. The channel dimensions are  $1000\text{ mm} \times 240\text{ mm} \times 60\text{ mm}$  ( $L \times W \times H$ ). Two vortex generators are arranged in a configuration where they share a flow direction and have an attack angle of 45 degrees. Located 170 mm downstream from the entrance of the channel.



(a) Geometry size of the channel and vortex generator pair



(b) Vortex generator

Figure 1. Physical model

**Table 1.** Geometric parameters of vortex generators

Type	$\alpha(^{\circ})$	$\beta(^{\circ})$	a(mm)	b(mm)	h(mm)	$\phi$ (mm)
DWP	26.6	45	40	0	20	-----
CDWP	26.6	45	40	10	20	-----
DWH	26.6	45	40	0	20	3
CDWH	26.6	45	40	10	20	3

## 2.2 Governing equations

The flow being simulated is steady and three-dimensional, and the air is considered to have constant properties and be incompressible. Depending on the Reynolds number, the flow could be either laminar or turbulent. The equations governing the flow do not take into account body force or viscous dissipation. These assumptions lead to the following written equivalences.

Continuity equivalence:

$$\frac{\partial u_j}{\partial x_j} = 0, (j=1, 2, 3) \quad (1)$$

Momentum balance for turbulent flow:

$$\frac{\partial u_j u_i}{\partial x_j} = \frac{\partial p}{\partial x_j} + \frac{\partial}{\partial x_j} \left( u \frac{\partial u_i}{\partial x_j} - \rho u_j^- u_i^- \right), (i, j = 1, 2, 3; i \neq j) \quad (2)$$

Energy equation:

$$\rho c_p u_j \frac{\partial T}{\partial x_j} = \frac{\partial y}{\partial x} \left( \lambda \frac{\partial T}{\partial x_j} \right), (j = 1, 2, 3) \quad (3)$$

## 2.3 Boundary conditions

As depicted in Figure 1(a), the velocity will be fully transferred through the inlet boundary condition.

$$T_{in} = 300 \text{ K at } x = 0, \frac{\partial u}{\partial z} = 0, w = v = 0 \quad (4)$$

At the outlet:

$$\frac{dT_f}{dx} = 0, \frac{\partial u}{\partial x} = \frac{\partial v}{\partial y} = \frac{\partial w}{\partial z} \quad (5)$$

The top, bottom, and side walls are subject to a no-slip boundary condition.

$$u = w = v = 0 \quad (6)$$

On the upper plane, an equal temperature is usually applied as:

$$T = T_s = 350 \text{ K} \quad (7)$$

The walls at the bottom and on the sides are regarded as walls that do not allow heat to pass through.

$$\left. \frac{\partial T}{\partial z} \right|_{z=H} = 0, \left. \frac{\partial T}{\partial z} \right|_{y=0} = 0 \quad (8)$$

The couple temperature is passed between LVG plane (solid) and nanofluid:

$$T_s = T_f \text{ and } k_s \left( \frac{\partial T}{\partial n} \right) \Big|_f = k_s \left( \frac{\partial T}{\partial n} \right) \Big|_s \quad (9)$$

In a state where  $n$  seems to be an average vector on the longitudinal vortex producer drawn out the edge.

The boundary condition for the symmetry plane can be written as:

$$\frac{\partial T}{\partial x} = \frac{\partial T_s}{\partial x} = 0, u = 0 \quad (10)$$

## 2.4 Solution method

The FLUENT CFD program was used to solve a mathematical model of an air channel that included vortex generators (VGs). The finite volume method was employed, together with a SIMPLE algorithm for connecting velocity and pressure. The structured grids used the Quick scheme, while the unstructured grids utilized the second upwind discretization. With Nusselt number deviations of less than 1.6%, there is going to be a concentration of thermal-hydraulic features through the plane rectangular VG pairs. This may confirm the merging of power equations stability, and motion, residuals of  $10^{-5}$ ,  $10^{-6}$ , and  $10^{-8}$  were used. The momentum and pressure below-relaxation components were placed at 0.3 and 0.7, respectively.

## 2.5 Dimensionless parameter

The Reynolds number (Re) may be summed and derived using the hydraulic diameter ( $D_h$ ) of the microchannel.

$$\text{Re} = \frac{\rho V_{in} D_h}{\mu}, D_h = \frac{2W.H}{W+H} \quad (11)$$

The hydraulic diameter is represented by  $D_h$ .

Using the relations below, the Nusselt number ( $Nu$ ) can be added:

$$Nu = \frac{h D_h}{k} \quad (12)$$

$$Q = \dot{m} c_p (T_{out} - T_{in}) \quad (13)$$

$$h = \frac{Q}{T_{wall} - \left( \frac{T_{in} + T_{out}}{2} \right)} \quad (14)$$

The mass flow is denoted by  $Q$ , which represents the total heat rate.

The apparent friction factor ( $f$ ) can be determined using the following equations.

$$f = \frac{2\Delta p}{\rho V_{in}^2} \times \frac{D_h}{L}, \Delta p = (p_{in} - p_{out}) \quad (15)$$

The amount of pressure can be dropped across the computational sphere as represented by  $\Delta p$ . where, Prandtl number is:

$$Pr = \frac{c_p \mu}{k} \quad (16)$$

Thermal performance of the system:

$$\eta = \left( \frac{Nu}{Nu_{bf}} \right) \left( \frac{f_{bf}}{f} \right)^{\frac{1}{3}} \quad (17)$$

### 3. VALIDATION AND MODEL VERIFICATION

#### 3.1 Grid independence test

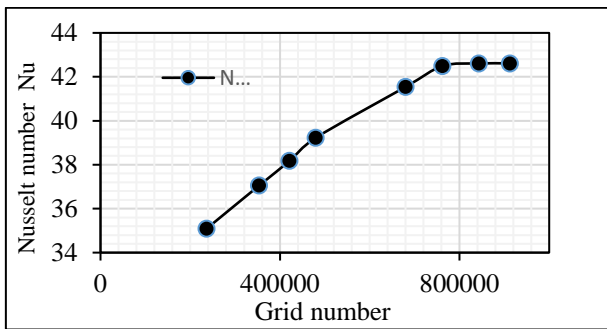
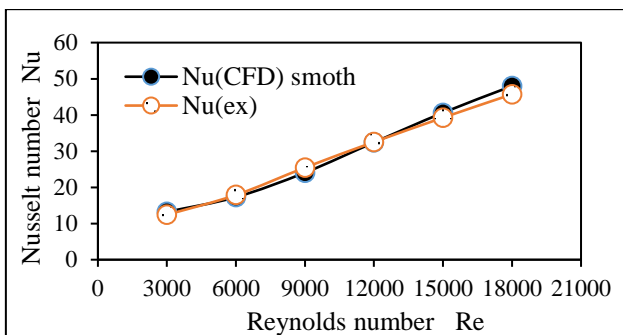
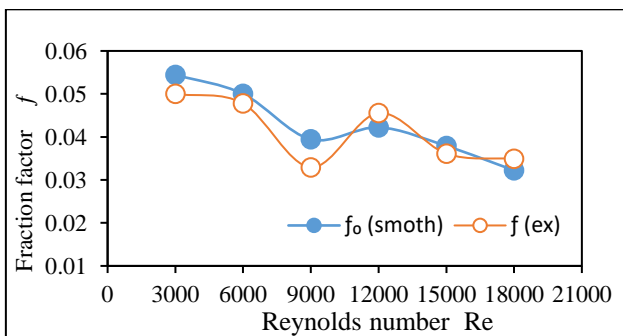


Figure 2. Grid independence test for CDWH (Re=12,000)



(a) Comparison of Num between the empirical correlations and the numerical results



(b) Comparison of  $f$  between the empirical correlations and the numerical results

Figure 3. The Model validation comparison of  $f$  and  $Num$

Different meshing techniques are used for fluid domains in a 3-D grid system. Unstructured tetrahedral elements are used for VGs with additional refinement for flow separation and secondary flows, while structured hexahedral grids are used for the rest of the channel domains. Grid independence tests are conducted using eight (32\*104, 35\*104, 42\*104, 47\*104, 67\*104, 76\*104, 84\*104, 91\*104) different grid numbers for the CDWH case with Re=12,000 and  $\alpha=45$ . Results show that

a grid number of 84\*104 and 91\*104 1.6% and 1.3%, respectively is sufficient with minimal differences in surface-average Num. Figure 2 displays the Num value that represents the average of the surface of the bottom channel wall.

#### 3.2 Model validation

Validation simulations were conducted based on the experimental findings of the winglet model, as reported by Zhou and Feng [19] and Nghaimesh [20]. The simulations were carried out in two different channels, one with a smooth surface and the other with a simple vortex generator (DWP), both at a Reynolds number of 12000. The maximum and minimum deviations observed were 8.4% and 3.7%, respectively, for the Nusselt number in the smooth channel. And the maximum and minimum deviations were 6.04% and 4.07%, respectively, for  $f$ . As depicted in Figure 3 (a), (b).

### 4. RESULTS AND DISCUSSIONS

#### 4.1 VGs with and without drilled holes are compared

The functions of the curved CDWP and CDWH and the plane VGs, DWP, and DWH. are presented in Figure 4. The VGs have a height-length ratio of  $h/l=1/2$  and are positioned at an attack angle of  $\beta=45$  degrees. For ease of explanation, the VGs with holes are referred to as H-series, while those without holes are called P-series. In the H-series, it is important to mention that the holes are punched at the center of VGs with a ratio of  $l/a$  being  $1/2$  and  $h'/h'$  being  $1/2$ . The ratio of the hole area to the VG area is 0.06. To assess the heat transfer enhancement, flow resistance, and overall performance of VGs, dimensionless factors such as  $Num/Num_0$ ,  $f/f_0$ , and  $R=(Num/Num_0)/(f/f_0)$  are utilized. Figure 4 shows a correlation between  $Num/Num_0$  and Re for planar vortex generators (VGs) in a channel stream. The results indicate that VGs with punched holes have higher  $Num/Num_0$  values compared to VGs without punched holes across all Re values. The most significant difference, up to 6.4%, is observed between VGs with openings (DWH) and VGs without punched holes (DWP) at Re=12,000. This improvement is due to the ability of the H-Series VGs openings to remove stagnant fluids behind the VGs, increasing kinetic energy in that region and leading to a rise in local intensity transfer. And displays the  $Num/Num_0$  with Re variation for curved VGs. Due to the smaller pressure differential before and after the curve VGs, the trend of  $Num/Num_0$  versus Re in Figure 4 is gentler and the value of  $Num/Num_0$  is slightly lower than that of the same type of plane VGs under identical Re. Followed by the marginally weaker vortex.

To indicate the drop in pressure the apparent resistance factor ( $f/f_0$ ) is utilized. According to Figure 5, the  $f/f_0$  initially increases rapidly and then stabilizes with Re. The DWP has the highest friction factor  $f/f_0$ , ranging from 1.1 to 1.7, owing to the greater area that confronts the airflow in the P-series of VGs, followed by DWH. The examined Re indicates that the H-series and that of VGs undergo less pressure deficit compared to the P-series of VGs. It becomes noticeable that the curved VGs CDW and CDWH have lower  $f/f_0$  than plane VGs because of their streamlined shape, resulting in less drag. This is so that the perforations' jet flow, which will result in the removal stationary fluids and reduce the pressure differentials by the VGs, can occur.

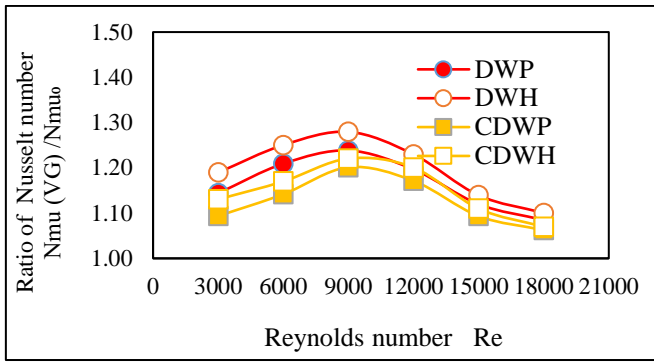


**Figure 4.** Comparison of VGs contains and without punched holes  $Nu/Num_0$

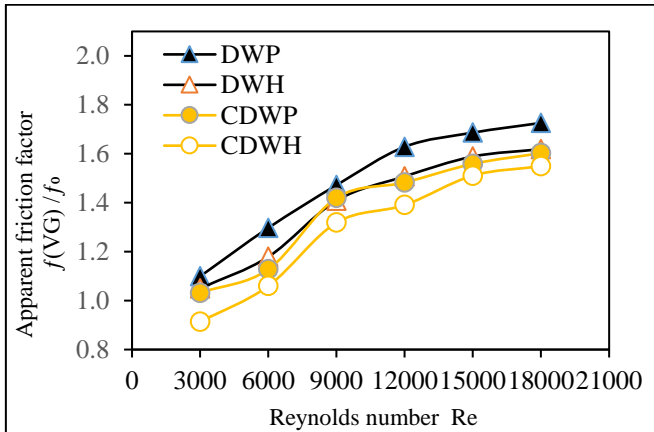


**Figure 5.** Comparison of VGs with and without punched holes  $f(VG)/f_0$

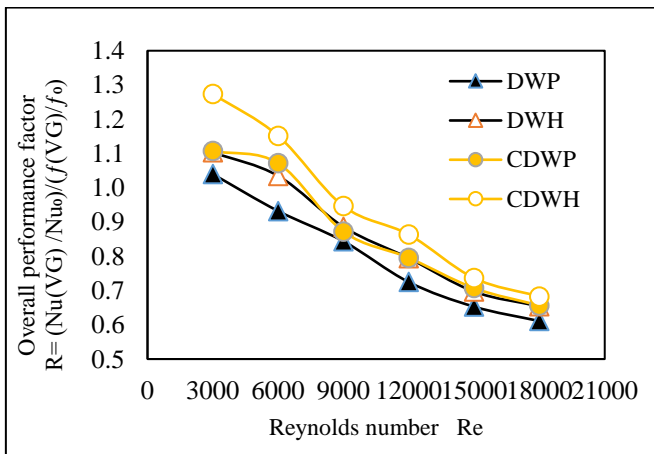


**Figure 6.** Comparison of VGs with and without punched holes  $(Nu(VG)/Nu_0)/(f(VG)/f_0)$

The thermal-hydraulic capacity R for each of these VGs' total flow regions is exhibited in Figure 6. The value of R falls as Re rises. Because of the combined effects of enhancing the transfer of heat and decreasing wire movement, the H series outperforms the P series for the identical VG shape. In contrast, the curved VG outperforms the corresponding flat VG.

#### 4.2 Thermal performance of the system

PEC will reduce while increasing Reynolds number. However, the PECs rates of the vortex generators in the lamellar region are comparable, the difference becomes more

pronounced in the turbulent region. The PEC is higher in (VG) with curved geometries and holes than without, especially at higher Reynolds numbers. The thermo-hydraulic efficiency coefficient consists of Colburn and friction coefficients, with CDWH having the most resistance, followed by CDWP, DWH, and DWP. At  $Re=18,000$ , the performance of the curved VG with holes outperforms that without, with a maximum difference of 35.3% shown in Figure 7.

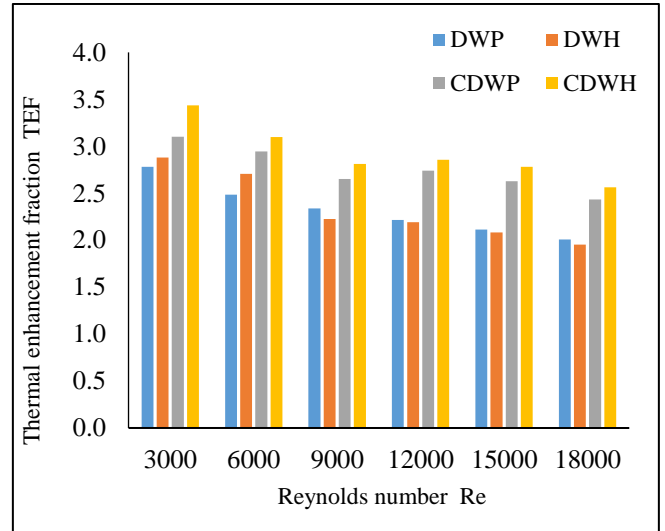


**Figure 7.** Numerical simulation results for TEF with the channel having curved VGs

#### 4.3 Comparison of various non-perforated vortex generator types

In most flow zones, curved winglet VGs promote heat transfer more effectively than flat winglet VGs, as demonstrated in Figure 8. As well as, CDWP ( $\alpha=20$ ) exhibits better thermal performance in totally turbulent and laminar zones. On the other hand, DWP shows the greatest values of  $j/j_0$  in transitional flow. The bigger fin area of curved winglets could be the reason for their better performance. Weaker heat transmission may also arise from the curved winglets' streamlined design, and this may reduce the flow splitting and reduce the recirculation domain after the VG. To validate this result, however, more investigation such as numerical simulation is necessary.

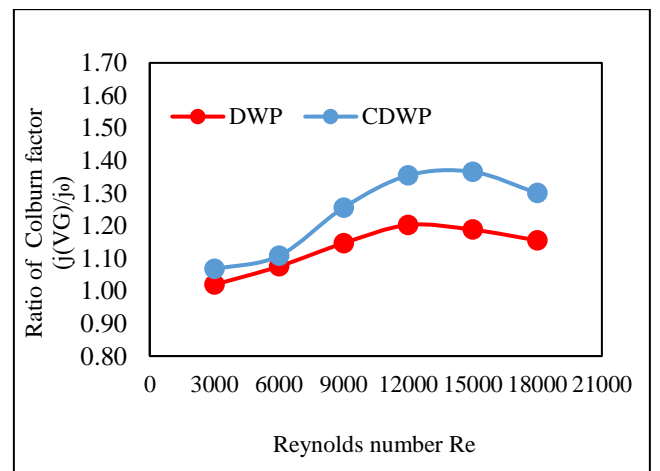


**Figure 8.** Comparison of various non-perforated vortex generator types

#### 4.4 Impact of punched hole diameter on VG performance

The good thermal function is achieved by VGs with fewer holes, such as CDWH and DWH, which have a smaller face area as shown in Figure 9. The most efficient hole diameter in laminar and provisional flow areas is found to be (3 mm) nevertheless, in total, there will be a reduction in violent flow, pierced holes that may reduce the transfer of heat in comparison to an empty flow. If there is a reduction in the wake zone, there may be two distinct outcomes, these are the pressure difference before and after the VG and the wake zone in which the punching zones may come up on the surface. Decreasing the pressure differential lessens the enhancement of heat transmission, whereas minimizing the wake zone enhances heat transfer. Because of this decreased face area of the CDWH, bigger holes (like 5 mm) in these VGs will lessen the already minimal pressure difference before and after the VG. Therefore, in certain situations, big holes might not be the best option for enhancing heat transfer.

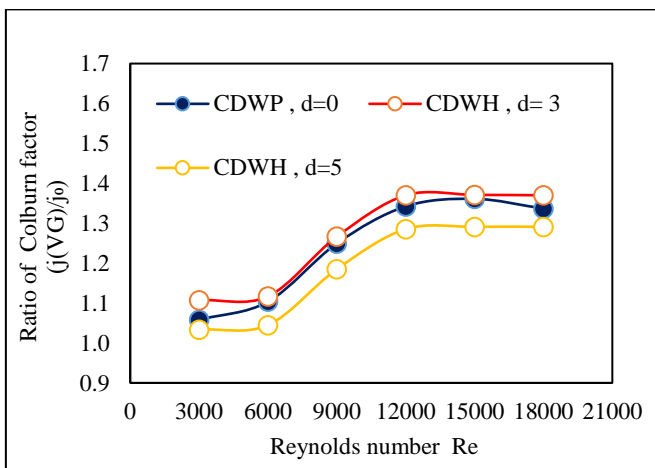


Figure 9. Impact of punched hole diameter on VG performance  $J(VG)/J_0$

#### 4.5 Velocity contour

The CFD as well as its topology of mean longitudinal speed has shown high values beyond the winglet which normally appears in pairs and distinct regions in regards to velocity variation behind it. The basic areas of the speed reduction are connected to the base of longitudinal vortices close to the section of every rectangular winglet. A related task is observed close to the symmetric axis after a distance of  $x/H=2$ , which shows the advancement of induced vortices. This close examination is in consonance with the practical findings explained by Oneissi et al. [21]. The results will exhibit symmetry when there is a transverse between the topologies of mean velocity constituents and that of experimental and numerical results. This may occur if the velocity constituent is placed behind the winglet pieces as a result of flow distribution.

The flow will be placed downward between the two various winglets and later be separated based on the two units. Here, the upwash flow will be shown in red while the downwash result in blue as well as the stagnation area. In this case, a major vortex will be generated owing to the separation on the winglet, which will rotate in a clockwise (CDW) direction and a tempted vortex counterclockwise (CDW) starts to exist after

a significant distance  $x/H=2$  from the winglet occurring from the end. From the winglet trailing edge. There is a noticeable agreement observed between experimental and numerical results, particularly, when analyzing turbulent kinetic energy. The SST turbulence model aligns well with the experimental output for the main vortex, especially with differences appearing much clearer beyond  $x/H$  higher than 3 as presented in Figure 10.

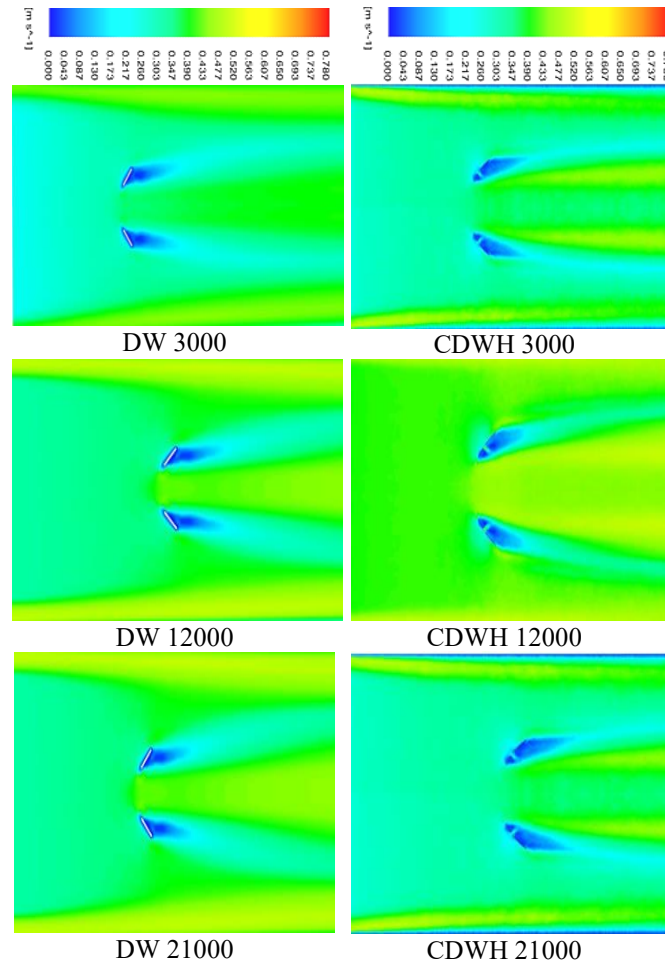
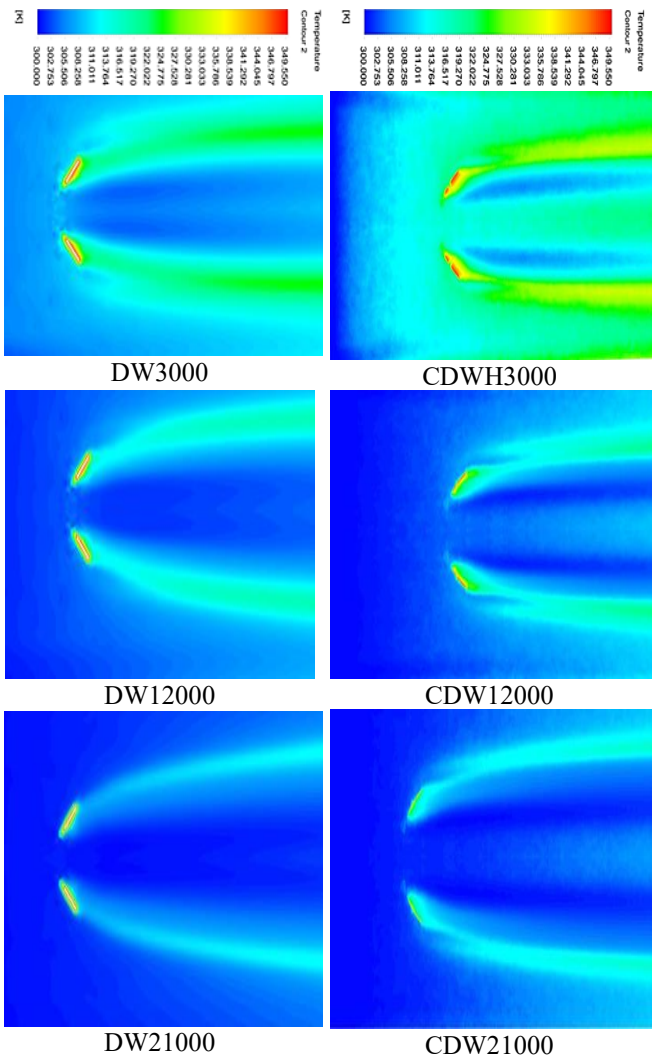


Figure 10. Velocity contour with VG

#### 4.6 Temperature contour

As a result of adiabatic conditions, the temperature variation will be weak around the channel. And it will be closely uniform in flow downstream from the inner part. Downstream of every LVG, the flow description will become blocked, with five (5) different units across the width. These units will become apparent at higher Re. The center of the jet close to the channel axis will form strong descending heat convection, as a result, it will elevate the temperature close to the axis. The widening of the central jet revolves the wake behind every LVG and leads to improved temperature close to axis. The growth of the main jet is restricted to the wake at each LVG, which leads to temperature advancement because of eddy mixture. The dimension of the separation bubble expands as a result of the increase in inlet speed. The eddy mixture behind each LVG. In this case, there will be a change, whereby the second pair of the LVG will become stronger than the initial pair as indicated in Figure 11.



**Figure 11.** Temperature contour with VG

## 5. CONCLUSIONS

In this study, we conducted 3-D mathematical simulations concerning channel movement with various VGs added to the lowest wall. Our analysis focused directly on heat transmission enactment and flow resistance of the VGs. The formation of tiny holes on the outer layer of VGs may enhance the transfer of heat and limit the resisting capacity of the flow. The examination of secondary velocity vectors and streamlines reveals a strong correlation between higher Nu and improved alignment between velocity vectors and temperature gradients. Furthermore, the usage of FSP can elucidate the underlying mechanism of heat transference improvement. For better heat dissipation, it is important to match the aperture area with the VG area. The ideal ratio of puncture force to VG power is currently 0.06, which is a product with an R-value of 0.69-1.23. This is much higher than VG without holes, which only has an R-value of 0.62-1.04. Piercing holes to the preceding edge and shortening the upright direction enhances heat transfer more effectively, however, there will be limited impact on flow resistance due to the position of the holes.

## REFERENCES

[1] Biswas, G., Chattopadhyay, H., Sinha, A. (2012).

Augmentation of heat transfer by creation of streamwise longitudinal vortices using vortex generators. *Heat Transfer Engineering*, 33(4-5): 406-424. <https://doi.org/10.1080/01457632.2012.614150>

[2] Lu, G., Zhou, G. (2016). Numerical simulation on performances of plane and curved winglet type vortex generator pairs with punched holes. *International Journal of Heat and Mass Transfer*, 102: 679-690. <https://doi.org/10.1016/j.ijheatmasstransfer.2016.06.063>

[3] Fiebig, M., Valencia, A., Mitra, N.K. (1993). Wing-type vortex generators for fin-and-tube heat exchangers. *Experimental Thermal and Fluid Science*, 7(4): 287-295. [https://doi.org/10.1016/0894-1777\(93\)90052-K](https://doi.org/10.1016/0894-1777(93)90052-K)

[4] Zhu, J.X., Fiebig, M., Mitra, N.K. (1995). Numerical investigation of turbulent flows and heat transfer in a rib-roughened channel with longitudinal vortex generators. *International Journal of Heat and Mass Transfer*, 38(3): 495-501. [https://doi.org/10.1016/0017-9310\(94\)00177-W](https://doi.org/10.1016/0017-9310(94)00177-W)

[5] Caliskan, S. (2014). Experimental investigation of heat transfer in a channel with new winglet-type vortex generators. *International Journal of Heat and Mass Transfer*, 78: 604-614. <https://doi.org/10.1016/j.ijheatmasstransfer.2014.07.043>

[6] Joardar, A., Jacobi, A.M. (2008). Heat transfer enhancement by winglet-type vortex generator arrays in compact plain-fin-and-tube heat exchangers. *International Journal of Refrigeration*, 31(1): 87-97. <https://doi.org/10.1016/j.ijrefrig.2007.04.011>

[7] Liu, C., Teng, J.T., Chu, J.C., Chiu, Y.L., Huang, S., Jin, S., Dang, T., Greif, R., Pan, H.H. (2011). Experimental investigations on liquid flow and heat transfer in rectangular microchannel with longitudinal vortex generators. *International Journal of Heat and Mass Transfer*, 54(13-14): 3069-3080. <https://doi.org/10.1016/j.ijheatmasstransfer.2011.02.030>

[8] Chen, C., Teng, J.T., Cheng, C.H., Jin, S., Huang, S., Liu, C., Lee, M.T., Pan, H.H., Greif, R. (2014). A study on fluid flow and heat transfer in rectangular microchannels with various longitudinal vortex generators. *International Journal of Heat and Mass Transfer*, 69: 203-214. <https://doi.org/10.1016/j.ijheatmasstransfer.2013.10.018>

[9] Chen, Y., Fiebig, M., Mitra, N.K. (1998). Heat transfer enhancement of a finned oval tube with punched longitudinal vortex generators in-line. *International Journal of Heat and Mass Transfer*, 41(24): 4151-4166. [https://doi.org/10.1016/S00179310\(98\)00130-6](https://doi.org/10.1016/S00179310(98)00130-6)

[10] Tiggelbeck, S., Mitra, N., Fiebig, M. (1994). Comparison of wing-type vortex generators for heat transfer enhancement in channel flows. *Journal of Heat Transfer*, 116(4): 880-885. <https://doi.org/10.1115/1.2911462>

[11] Lu, G., Zhou, G. (2016). Numerical simulation on performances of plane and curved winglet-Pair vortex generators in a rectangular channel and field synergy analysis. *International Journal of Thermal Sciences*, 109: 323-333. <https://doi.org/10.1016/j.ijthermalsci.2016.06.024>

[12] Torii, K., Kwak, K.M., Nishino, K. (2002). Heat transfer enhancement accompanying pressure-loss reduction with winglet-type vortex generators for fin-tube heat exchangers. *International Journal of Heat and Mass Transfer*, 45(18): 3795-3801. [https://doi.org/10.1016/S0017-9310\(02\)00080-7](https://doi.org/10.1016/S0017-9310(02)00080-7)

[13] Saini, P., Dhar, A., Powar, S. (2023). Performance

- enhancement of fin and tube heat exchanger employing curved delta winglet vortex generator with circular punched holes. *International Journal of Thermofluids*, 20: 100452. <https://doi.org/10.1016/j.ijft.2023.100452>
- [14] Wang, J., Zeng, L., Fu, T., Yu, S., He, Y. (2024). Effects of the position and perforation parameters of the delta winglet vortex generators on flow and heat transfer in minichannels. *International Journal of Thermal Sciences*, 198: 108878. <https://doi.org/10.1016/j.ijthermalsci.2023.108878>
- [15] Wu, J., Tao, W. (2012). Effect of longitudinal vortex generator on heat transfer in rectangular channels. *Applied Thermal Engineering*, 37: 67-72. <https://doi.org/10.1016/j.applthermaleng.2012.01.002>
- [16] Zhou, G., Feng, Z. (2014). Experimental investigations of heat transfer enhancement by plane and curved winglet type vortex generators with punched holes. *International Journal of Thermal Sciences*, 78: 26-35. <https://doi.org/10.1016/j.ijthermalsci.2013.11.010>
- [17] Tian, L.T., He, Y.L., Lei, Y.G., Tao, W.Q. (2009). Numerical study of fluid flow and heat transfer in a flat-plate channel with longitudinal vortex generators by applying field synergy principle analysis. *International Communications in Heat and Mass Transfer*, 36(2): 111-120. <https://doi.org/10.1016/j.icheatmasstransfer.2008.10.018>
- [18] Lin, Z.M., Liu, C.P., Lin, M., Wang, L.B. (2015). Numerical study of flow and heat transfer enhancement of circular tube bank fin heat exchanger with curved delta-winglet vortex generators. *Applied Thermal Engineering*, 88: 198-210. <https://doi.org/10.1016/j.applthermaleng.2014.11.079>
- [19] Zhou, G., Feng, Z. (2014). Experimental investigations of heat transfer enhancement by plane and curved winglet type vortex generators with punched holes. *International Journal of Thermal Sciences*, 78: 26-35. <https://doi.org/10.1016/j.ijthermalsci.2013.11.010>
- [20] Nghaimesh, S.J. (2024). Study of the effect of curve-type vortex generator pairs with perforated and flat holes on airfoil performance. *Nanotechnology Perceptions*, 20(S2): 175-191. <https://doi.org/10.62441/nano-ntp.v20iS2.15>
- [21] Oneissi, M., Habchi, C., Russeil, S., Bougeard, D.,

Lemenand, T. (2016). Novel design of delta winglet pair vortex generator for heat transfer enhancement. *International Journal of Thermal Sciences*, 109: 1-9. <https://doi.org/10.1016/j.ijthermalsci.2016.05.025>

## NOMENCLATURE

H	channel height (mm)
$f_0$	the friction factor of a smooth channel
T	temperature (K)
S	front edge pitch of a pair of vortex generators (mm)
D	the hydraulic diameter of the air channel (mm)
h	height of vortex generator (mm)
Q	heat transfer rate (W)
j	colburn factor
$j_0$	the Colburn factor of the smooth channel (i.e. without VG)
d	hole diameter (mm)
p	pressure (Pa)
C <sub>p</sub>	specific heat (J kg <sup>-1</sup> C <sup>-1</sup> )
U	velocity profile
P <sub>in</sub>	the pressure of the inlet (Pa)
CDWH	curved delta winglet pair with holes
L	channel length (mm)
Nu	nusselt number
Nu <sub>0</sub>	Nusselt number of smooth channels
pr	prandtl number
D <sub>p</sub>	pressure drop (Pa)
Re	reynolds number
R	overall performance factor $(Nu/Nu_0)/(f/f_0)$
DWH	delta winglet pair with holes
DWP	delta winglet pair
CDWP	curved delta winglet pair

## Greek letters

$\alpha$	inclination angle of LVGs (°)
$\beta$	attack angle (°)
$\phi$	ratio of hole area to VG area
$\rho$	density (kg m <sup>-3</sup> )
$f$	fraction factor